Rationally Designed Gibbous Stimuli-Responsive Colloidal Nanoparticles

Chunliang Lu and Marek Urban*

Department of Materials Science and Engineering, Center for Optical Materials and Engineering Technologies (COMSET), Clemson University, Clemson, South Carolina 29634-0915, United States

ABSTRACT Multiphase colloidal copolymer nanoparticles, if properly designed, offer a number of unique properties and well-documented technological opportunities for drug delivery, nanolithography, high surface area colloidal crystals, or hollow nanoparticles, to name just a few. Using a simple free radical polymerization process, we synthesized copolymer nanoparticles with controlled stimuli-responsive phase-separated gibbosities. The topography of the gibbous phase can be controlled by the copolymer composition and polymerization conditions. When pH-sensitive monomers were copolymerized onto surface bulges, pH changes resulted in localized gibbous phase dimensional changes. Facilitated by monomer diffusion into interfacial particle seed solution regions, localized polymerization near the surface is responsible for the formation of phase-separated gibbous topographies. This general approach may offer a number of possibilities for controllable design of ordered heterogeneous copolymer morphologies for a variety of applications.

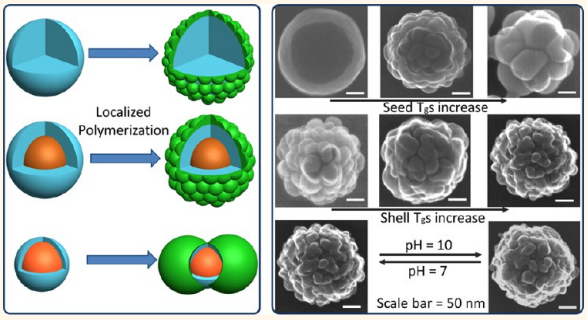

KEYWORDS: gibbous colloidal nanoparticles · "raspberry" particle morphology control · stimuli-responsive nanoparticles · inorganic–organic composite colloids

Processes occurring in nature lead to a variety of heterogeneous morphologies with often amazing shapes at various length scales. While mimicking molecular events leading to the formation of different shapes and scaled-up morphologies is challenging, recent attempts successfully showed that an interplay of dynamic reactions combined with diffusion processes may facilitate the growth of well-defined, complex, and unique microstructures.[1,2] The challenge is to facilitate desirable thermodynamic and kinetic conditions that will lead to controllable heterogeneities and anisotropies.[3−6] At nanoscales, these challenges are amplified by the limited ability to measure highly localized events at or near inter- and intramolecular bond scales.[7] Although previous studies have developed irregular nanoparticles utilizing electrostatic forces,[8,9] emulsion–evaporation,[10,11] hydrogen bonding,[12] capillary forces,[13] covalent bonding,[14−16] or acid–base interactions,[17,18] the precise control of chemicophysical events facilitating hierarchical buildups leading to highly organized 3D arrays[19,20] with stimuli-responsive attributes has not been shown. Although triphasic stimuli-responsiveness Janus nanoparticles were prepared,[7] controllable stimuli-responsive nanoparticle gibbosity has not been exploited. In these studies, we developed colloidal nanoparticles with tunable gibbousness that change size upon pH environmental changes. These materials may offer numerous future opportunities for technological advances in the areas where high surface-to-volume properties are needed, such as multistage drug delivery systems, nanoporous materials for energy storage, thermal barrier materials, or remarkably high surface area catalysts with high yields, just to name a few; there are others.

RESULTS AND DISCUSSION

Synthesis of gibbous nanoparticles consists of three steps: (1) synthesis of a seed, (2) swelling the seed with monomers, followed by (3) polymerization of the monomers swollen in the seed. Figure 1 illustrates how nanoparticle morphologies are controlled by minute modifications of reaction conditions. For example, TEM images in Figure 1a–d illustrate the seeds which may consist of a homopolymer, such as

* Address correspondence to mareku@clemson.edu.

Received for review December 31, 2014 and accepted February 19, 2015.

Published online February 19, 2015
10.1021/nn507489p

pMMA (a), or an inorganic core and polymer shell, such as SiO_2-pMMA core−shell nanoparticles with shell thicknesses of ~10, 30, and 100 nm (b−d). TEM images in Figure 1a′/a″/a‴ illustrate particle morphologies resulting from copolymerization of pentafluorostyrene/*n*-butyl acrylate (PFS/nBA, wt ratio = 2:1; molar ratio = 1.32:1) with various feed amounts in the presence of pMMA seed particles. As shown, a large number of protuberances are produced, and as the monomer feed amount increases, fewer but larger protuberances are formed. The series of TEM images b′/b″/b‴−d′/d″/d‴ illustrate the morphology changes of the inorganic−organic core−shell gibbous particles as a function of monomer feed amount as well as the shell thickness of SiO_2-pMMA seed particles. When the pMMA shell thickness of the seed particles is >30 nm, as shown in Figure 1c′/c″c‴,d′/d″/d‴, gibbous nanoparticles containing well-spaced and round protuberances are formed, and as the monomer feed amount increases, the number of protuberances decreases while the size increases, which is confirmed by the SEM images shown in Supporting Information Figure S2. The composition of core−shell gibbous particles is also manifested by the SEM images and the corresponding spatial elemental analysis of nanoparticles in Figure S3. It can be seen that the silica core is not involved in this process. However, when the pMMA shell thickness is ~10 nm, as shown in Figure 1b″, copolymerization of 144 mM PFS/nBA results in anisotropic particles with three or four bulges on the surface. A 2-fold increase of the monomer feed (288 mM) results in dumbbell-like (two bulges) morphologies (Figure 1b‴).

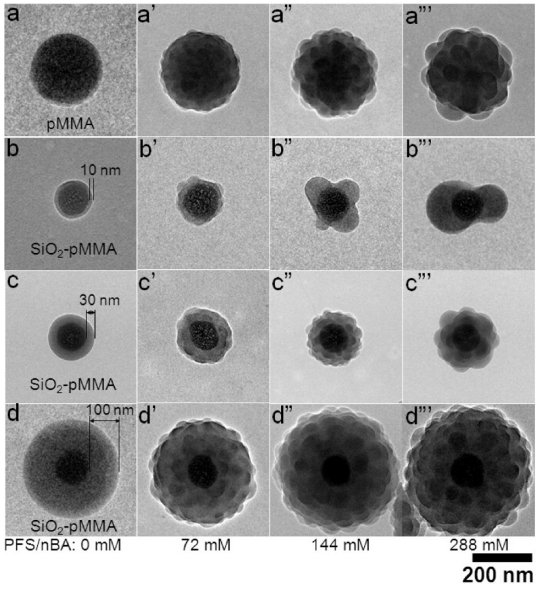

Figure 1. TEM images of pMMA seed (~250 nm) (a) and SiO_2-pMMA seed nanoparticles with a shell thickness of ~10 (b), 30 (c), and 100 nm (d); TEM images a′−d′, a″−d″, and a‴−d‴ represent individual nanoparticles synthesized by the swelling and polymerization process using PFS/nBA monomers. TEM images a′−a‴/b′−b‴/c′−c‴/d′−d‴ correspond to the following monomer feed amounts (PFS/nBA, molar ratio = 1.32:1): 72, 144, and 288 mM, respectively. Figure S1 of the Supporting Information illustrates TEM images of larger populations of the same nanoparticles.

In view of these data, two questions need to be addressed: what drives the formation of gibbosity, and what are the molecular processes responsible for this behavior. For that reason, we extracted aliquots during polymerization and conducted the particle size analysis (Figure S4). The particle size rapidly increases during the first 10 min of polymerization from 250 to 297 nm, to reach the maximum at ~318 nm after 120 min. As shown in Figure 2a, pMMA seed particles are uniform compositionally and topographically. As PFS/nBA monomers swell pMMA, their surface softens, as shown in Figure 2b. As polymerization is initiated

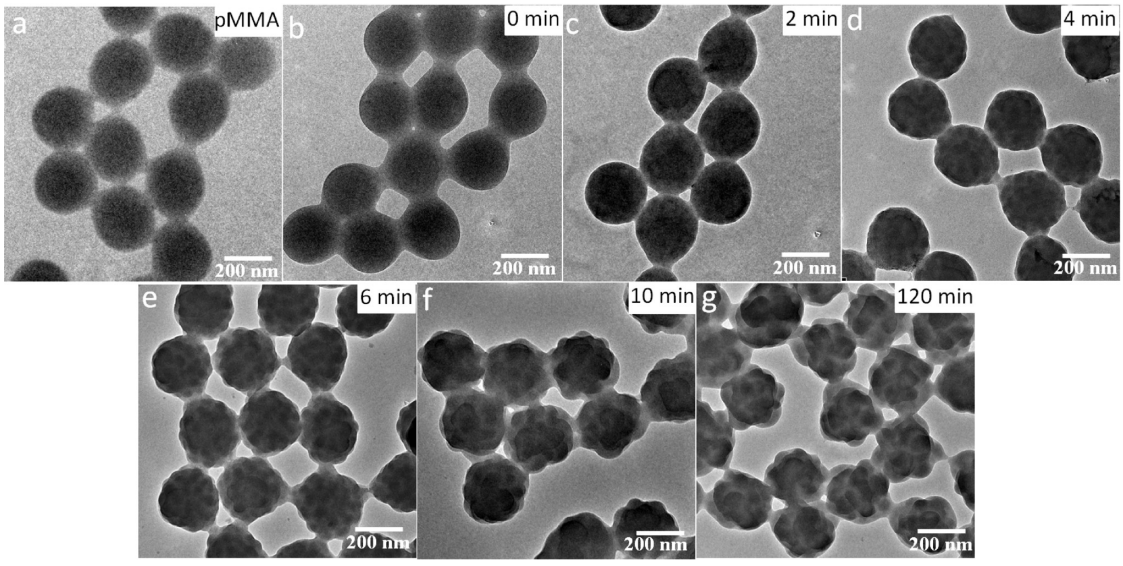

Figure 2. Morphologies developed during swelling and polymerization of 288 mM PFS/nBA (molar ratio = 1.32:1) in the presence of pMMA seeds (a) as a function of polymerization time: 0 (b), 2 (c), 4 (d), 6 (e), 10 (f), and 120 min (g).

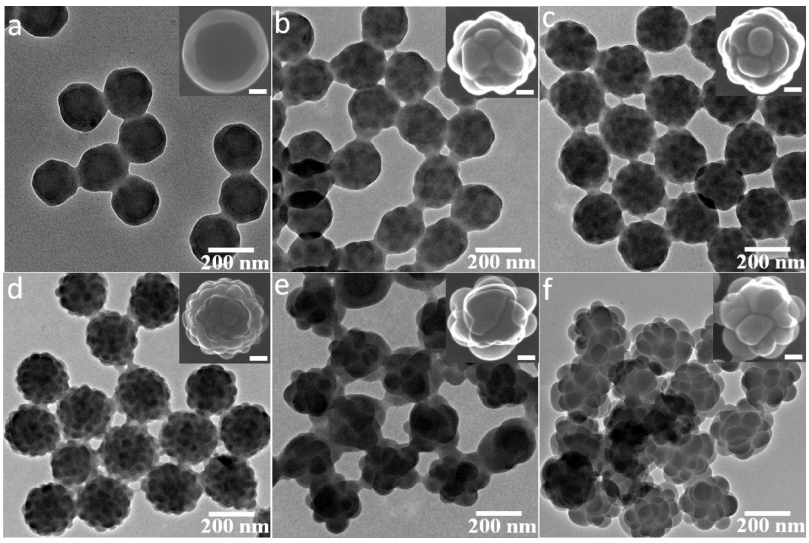

Figure 3. TEM images of gibbous nanoparticles synthesized by utilizing 144 mM PFS/nBA (1.32:1 molar ratio) in the presence of p(MMA/nBA) seeds (particle size 250 ± 5 nm) with T_g values of ~50 (a), 75 (b), 90 (c), and 105 °C (d) and p(MMA/MAA) seeds (particle size 250 ± 5 nm) with the T_g values of ~114 (e) and 117 °C (f). The insets are SEM images of respective nanoparticles. Scale bar is 50 nm.

after 2 min, phase-separated regions are formed (Figure 2c), which become larger and spherical (4 min). At the same time, bulges begin to form and after 6 min become larger, but their quantities remain constant. As polymerization continues (10−120 min), the size of the bulges keeps increasing and adjacent phase-separated bulges may merge into a larger bulge. During this process, it can be seen that both the deformation of seed particles and bulges play an important role in gibbous morphology formation.

The role of deformability of seeds was examined by tuning the T_g of p(MMA/nBA) and p(MMA/methacrylic acid(MAA)) particles. TEM images shown in Figure 3a−d illustrate images of resulting gibbous particle from p(MMA/nBA) seed particles with the T_g of 50 to 75, 90, and 105 °C and show that protuberances are more pronounced at higher T_g values. As a matter of fact, seed nanoparticles with the $T_g < T_P$ (T_P is polymerization temperature) will lead to core−shell inversion, as demonstrated in Figure 3a and predicted in earlier studies.[21] When the T_g of the core is ~75 °C, protuberances form (Figure 3b), and when $T_g > T_P$, gibbosity is produced (Figure 3c,d). Similar morphologies are observed when pMMA/nBA-SiO_2 seed particles are utilized (Figure S5). As the T_g of the seed further increases, by copolymerizing MMA with MAA to 114 and 117 °C, significantly larger protuberances are produced.

The role of mobility for growing fluorinated polymer chains on the gibbosity formation was examined by tuning p(PFS/nBA) (or p(PFS/MAA)) to desired T_g values. As shown in Figure 4a, when the PFS/nBA ratio is 1:1, the resulting copolymers exhibit $T_g = -5$ °C, below room temperature, and no bulges are formed due to enhanced chain mobility. As the PFS/nBA ratio increases to 1.5:1 and the T_g of the resulting copolymers (25 °C) reaches room temperature, bulges begin to form (Figure 4b). More pronounced bulges are formed with the increase of PFS/nBA ratio (Figure 4c). However, when only PFS monomer (T_g = 80 °C) or PFS/MMA (wt ratio 10:1, T_g = 82 °C) is utilized, irregular protuberances with sharp edges are formed (Figure 4d,e). Further increase of the T_g to 102 °C results in the formation of a significantly greater number of small bulges, which is likely due to the restricted mobility of phase-separated copolymer regions.

On the basis of these experimental results, the following mechanism of the gibbosity development in nanoparticles is proposed. As depicted in Figure 5a1, at a given polymerization temperature, hydrophilic initiator-derived radicals approach seed particle surfaces to initiate polymerization of monomers (PFS and nBA) near the surface. Upon initiation, polymerization continues as long as monomer supplies last and hydrophobic bulges are formed. Their growth is driven by a greater surface tension difference between p(PFS/nBA) and water than that between the seed and aqueous phase (Table S1). At the same time, the limited free volume within the seed inhibits diffusivity of p(PFS/nBA) chains' inward particles. As a result, they form protuberances on seed nanoparticle surfaces (Figure 5a2). Another driving force for supplying monomers to the seed particle surface is the higher solubility of reactive monomers in copolymerized protuberances compared to the seed (Figure 5a3). As polymerization proceeds, the protuberances form gibbous surfaces (Figure 5a4). The same process is responsible for the formation of protuberances when SiO_2-pMMA particles with a thick pMMA shell (>20 nm) are utilized as seeds (Figure 5b). However, when SiO_2-pMMA has a thin pMMA shell (~10 nm), seeded

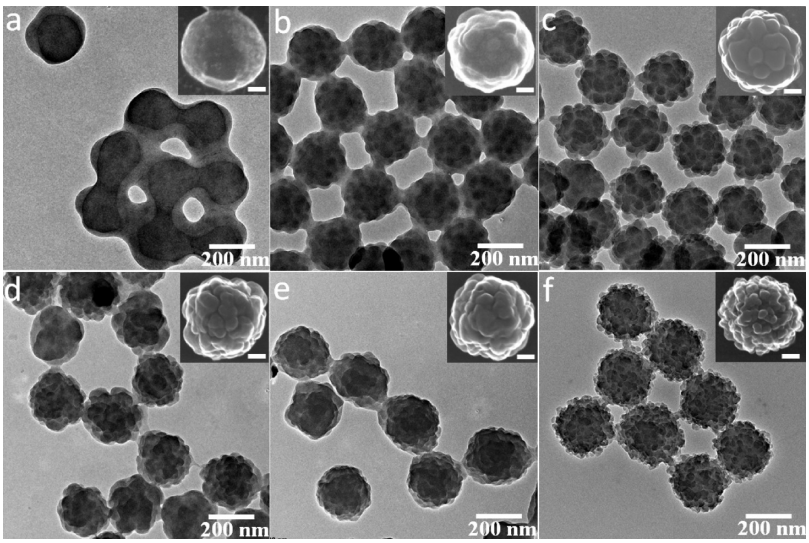

Figure 4. TEM images of nanoparticles obtained by swelling polymerization of PFS/nBA with weight ratios of 1:1 (a), 1.5:1 (b), 11:1 (c), and 1:0 (d) and of PFS/MMA with weight ratio of 10:1 (e) and PFS/MAA weight ratio of 10:1 (f) in the presence of pMMA seeds (particle size ~250 ± 5 nm). The copolymer shells have estimated T_g values of −5, 25, 60, 80, 82, and 102 °C, respectively. The insets are SEM images of respective nanoparticles. Scale bar is 50 nm.

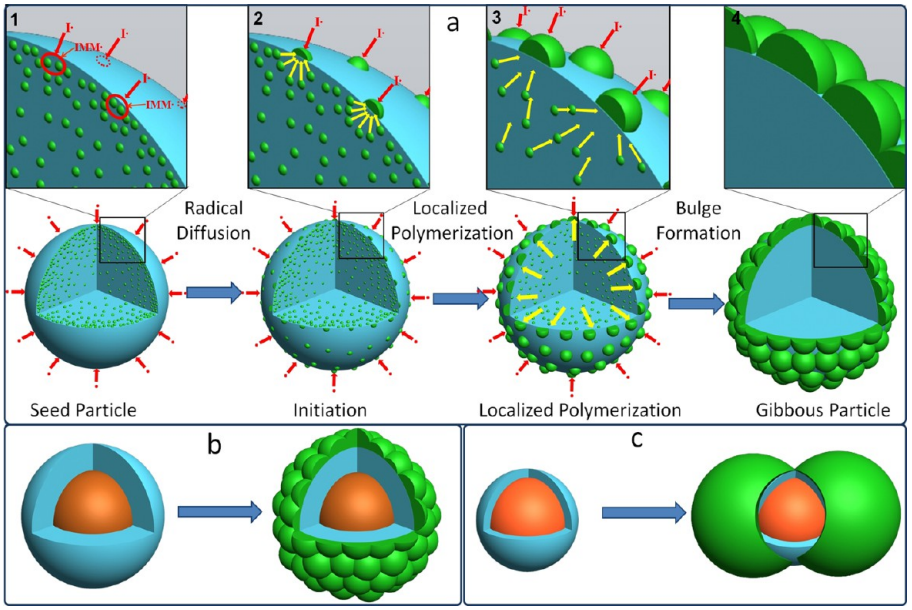

Figure 5. Schematic representation of the mechanism responsible for the formation of raspberry-like morphologies by seeded emulsion polymerization (a) and representation of the formation of core−shell raspberry-like (b) and dumbbell-like (c) particles.

emulsion polymerization results in the formation of particles with fewer protuberances as well as dumbbell-shaped particles (Figure 5c). Since the pMMA layer is not sufficiently thick, adjacent growing protuberances merge to form two protuberances on opposite sides of the core, resulting in dumbbell-shaped particles.

The gibbous particles containing MAA components exhibit different surface topographies at neutral and basic conditions. As shown in Figure 6a, at pH = 7, the particles exhibit a large number of small bulges with fairly distinct edges. However, when pH = 10, carboxylic acid groups of pMAA side chains are deprotonated, thus carrying negative charges along the copolymer backbone. As a result, the overall diameter of the gibbous particles increases from 260 to 290 nm (Figure 6) due to expansion, manifested by the development of rounded edges. In an effort to illustrate the size changes of the bulges, each SEM image of Figure 6 shows magnified individual bulges as a function of pH. On average, the bulge diameter increases by ~15%. To further justify the stimuli-responsiveness and stability of gibbous nanoparticles, ζ-potential measurements were conducted as a function of pH. The results are shown in Figure S8 of the Supporting Information, which illustrates ζ-potential and particle size changes plotted as a function of pH. As seen, when the degree of

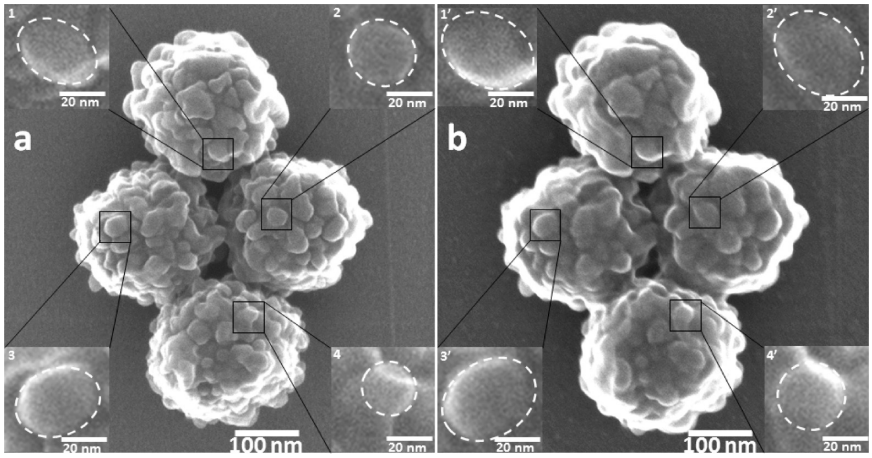

Figure 6. SEM images of p(MMA-PFS/MAA) gibbous particles at pH 7 (a) and pH 10 (b). The insets are magnified SEM images of a bulge at respective pH (scale bar = 20 nm).

neutralization increases, ζ-potential values decrease, which parallels the particle increase. The apparent dissociation constant (pK_a) of the poly(methacrylic acid) component is ~3.6,[22] and Figure S8 clearly illustrates that above that value ζ-potential levels off at approximately −40−45 mV, thus stabilizing the particles, which parallels their size increase.

CONCLUSION

Gibbous nanoparticles with controlled morphologies and surface topographies were synthesized *via* seeded emulsion polymerization. The gibbosity of the particles can be easily controlled by altering monomer composition/concentration. Furthermore, incorporation of pH-responsive components into the bulges results in stimuli-responsiveness manifested by size changes under different pH conditions. These controlled heterogeneous topographies will lead to the development of complex, high surface colloidal crystals with lowest symmetries, an opportunity for entrapment of nano-objects inside gibbous cavities and others.

EXPERIMENTAL SECTION

Materials. Tetraethoxysilane (TEOS) and ammonium hydroxide (28−32% in water), methyl methacrylate (MMA), *n*-butyl acrylate (nBA), *t*-butyl acrylate (tBA), styrene (St), methacrylic acid (MAA), pentafluorostyrene (PFS), potassium persulfate (KPS), 3-(methacryloyloxy)propyl trimethoxysilane (MPS), and aluminum oxide (Al_2O_3) were purchased from Aldrich Chemical Co. MMA, nBA, MAA, St, and PFS were allowed to pass through an Al_2O_3 column to remove inhibitors prior to use, and all other chemicals were used as received.

Preparation of p(MMA/nBA), p(MMA/MAA), or pSt Particles by Surfactant-Free Emulsion Polymerization. Ninety milliliters of deionized water (H_2O, 5 mol) was added into a reaction flask maintained at 75 °C, purged continuously with N_2 gas, and stirred mechanically at 400 rpm. Three grams of MMA/nBA (or MMA/MAA, St) monomer mixture and 5 mL of KPS aqueous solution (0.01 g/mL, 37 mM) were added, and the reaction was allowed to continue for 5 h (15 h for pSt to ensure full conversion). The seed particles were purified by centrifugation at 1500*g* for 3 h. Upon completion, they were redispersed in 95 mL of deionized water. Monomer molar ratios, particle sizes, and % monomer conversions are listed in Table S2 of the Supporting Information.

Preparation of Silica Particles. The colloidal silica particles were synthesized according to the well-known Stöber method.[23] Ten grams of TEOS (0.048 mol), 200 mL of absolute ethanol (3.43 mol), and 10 mL of ammonium hydroxide (0.09 mol) were introduced into a 500 mL round-bottom flask while being stirred at 350 rpm at room temperature for 24 h. The colloidal dispersion was purified by repeated centrifugation redispersion cycles with deionized water for more than three times. The final SiO_2 particles (particle size ~95 nm) were collected by centrifugation at 1000*g* for 3 h (63% yield).

Preparation of SiO_2-pMMA Core−Shell Nanoparticles. The surface of MPS silica particles (95 nm) was modified by MPS to attach a C═C double bond, which facilitates the formation of SiO_2-pMMA core−shell nanoparticles. Sixty milliliters of colloidal silica dispersion (0.5 w/w%) was added into a reaction flask maintained at 75 °C, purged continuously with N_2 gas, and stirred mechanically at 350 rpm. Then 0.6 mL of 1% KOH aqueous solution (0.107 mmol) was introduced into the colloidal dispersion. Thirty minutes later, 0.07 g of MPS (0.28 mmol) was added dropwise into the flask to modify the silica particle surface with methacrylate groups. The monomer MMA and KPS initiator were continuously fed into the system over 2 h, and the reaction was continued for 5 h. The seed particles were purified by centrifugation at 1000*g* for 3 h and redispersed in 65 mL of deionized water. Table S3 of the Supporting Information provides a list of synthesized particles, monomers, initiator feed amounts, and % monomer conversions.

Preparation of Gibbous Composite Particles. Monomers (compositions shown in Table S4 in the Supporting Information) were added into 5 g seed particle dispersions stirred at 600 rpm. After the monomers completely diffused into the seed particles (over 15 h), the colloidal dispersion was deoxygenated by purging N_2 for 30 min, and KPS aqueous solution (feed amounts shown in Table S4) was added. The reaction was continued for 2 h at 75 °C. The gibbous particles synthesized using this procedure are monodispersed, and agglomerates/aggregates are rarely observed. No separation was needed for TEM/SEM experiments. Monomer compositions, KPS feed amounts, and conversions are listed in Table S4.

Characterization. Particle size measurements were performed using a Malvern Zetasizer Nano ZS at 25 °C. Particle morphologies were examined using a Hitachi H9500 transmission electron microscope (TEM) operated at 300 kV and a Hitachi

HD2000 scanning transmission electron microscope (STEM) with energy-dispersive X-ray spectroscopy function operated at 200 kV. Each colloidal dispersion at ~5 w/w % solids, upon 1:10^4 dilution, was deposited on a carbon film Cu grid (EMS), and TEM and SEM analyses were performed. The pH-responsiveness of pMMA-p(PFS/MAA) nanoparticles was determined by depositing the diluted nanoparticles on a carbon film Cu grid, and initial SEM analysis was performed. In the next step, the specimen was dipped into an aqueous solution of KOH (0.1 mM; pH = 10) for 30 min. Upon removal and drying for 30 min, the same SEM analysis was repeated (Figure 6).

Conflict of Interest: The authors declare no competing financial interest.

Acknowledgment. This work was partially supported by the National Science Foundation under Award CMMI 1332964 and J.E. Sirrine Foundation Endowment at Clemson University.

Supporting Information Available: Additional experimental figures, tables, and characterizations. This material is available free of charge *via* the Internet at http://pubs.acs.org.

REFERENCES AND NOTES

1. Noorduin, W. L.; Grinthal, A.; Mahadevan, L.; Aizenberg, J. Rationally Designed Complex, Hierarchical Microarchitectures. *Science* **2013**, *340*, 832–837.
2. Mitragotri, S.; Lahann, J. Physical Approaches to Biomaterial Design. *Nat. Mater.* **2009**, *8*, 15–23.
3. Wang, Y.; Wang, Y.; Breed, D. R.; Manoharan, V. N.; Feng, L.; Hollingsworth, A. D.; Weck, M.; Pine, D. J. Colloids with Valence and Specific Directional Bonding. *Nature* **2012**, *491*, 51–55.
4. Kraft, D. J.; Vlug, W. S.; van Kats, C. M.; van Blaaderen, A.; Imhof, A.; Kegel, W. K. Self-Assembly of Colloids with Liquid Protrusions. *J. Am. Chem. Soc.* **2008**, *131*, 1182–1186.
5. Oh, M.; Mirkin, C. A. Chemically Tailorable Colloidal Particles from Infinite Coordination Polymers. *Nature* **2005**, *438*, 651–654.
6. Caruso, F. Nanoengineering of Particle Surfaces. *Adv. Mater.* **2001**, *13*, 11–22.
7. Lu, C.; Urban, M. W. Tri-phasic Size- and Janus Balance-Tunable Colloidal Nanoparticles (JNPs). *ACS Macro Lett.* **2014**, *3*, 346–352.
8. Caruso, F.; Caruso, R. A.; Möhwald, H. Nanoengineering of Inorganic and Hybrid Hollow Spheres by Colloidal Templating. *Science* **1998**, *282*, 1111–1114.
9. Hong, L.; Cacciuto, A.; Luijten, E.; Granick, S. Clusters of Charged Janus Spheres. *Nano Lett.* **2006**, *6*, 2510–2514.
10. Cho, Y.-S.; Yi, G.-R.; Lim, J.-M.; Kim, S.-H.; Manoharan, V. N.; Pine, D. J.; Yang, S.-M. Self-Organization of Bidisperse Colloids in Water Droplets. *J. Am. Chem. Soc.* **2005**, *127*, 15968–15975.
11. Manoharan, V. N.; Elsesser, M. T.; Pine, D. J. Dense Packing and Symmetry in Small Clusters of Microspheres. *Science* **2003**, *301*, 483–487.
12. Li, R.; Yang, X.; Li, G.; Li, S.; Huang, W. Core-Corona Polymer Composite Particles by Self-Assembled Heterocoagulation Based on a Hydrogen-Bonding Interaction. *Langmuir* **2006**, *22*, 8127–8133.
13. Li, F.; Stein, A. Conjugation of Colloidal Clusters and Chains by Capillary Condensation. *J. Am. Chem. Soc.* **2009**, *131*, 9920–9921.
14. Ming, W.; Wu, D.; van Benthem, R.; De With, G. Superhydrophobic Films from Raspberry-like Particles. *Nano Lett.* **2005**, *5*, 2298–2301.
15. Puretskiy, N.; Ionov, L. Synthesis of Robust Raspberry-like Particles Using Polymer Brushes. *Langmuir* **2011**, *27*, 3006–3011.
16. Qian, Z.; Zhang, Z.; Song, L.; Liu, H. A Novel Approach to Raspberry-like Particles for Superhydrophobic Materials. *J. Mater. Chem.* **2009**, *19*, 1297–1304.
17. Cheng, X.; Chen, M.; Zhou, S.; Wu, L. Preparation of SiO_2/PMMA Composite Particles *via* Conventional Emulsion Polymerization. *J. Polym. Sci., Part A: Polym. Chem.* **2006**, *44*, 3807–3816.
18. Chen, M.; Wu, L.; Zhou, S.; You, B. Synthesis of Raspberry-like PMMA/SiO_2 Nanocomposite Particles *via* a Surfactant-Free Method. *Macromolecules* **2004**, *37*, 9613–9619.
19. Sacanna, S.; Irvine, W.; Chaikin, P. M.; Pine, D. J. Lock and Key Colloids. *Nature* **2010**, *464*, 575–578.
20. Wang, Y.; Wang, Y.; Zheng, X.; Yi, G.-R.; Sacanna, S.; Pine, D. J.; Weck, M. Three-Dimensional Lock and Key Colloids. *J. Am. Chem. Soc.* **2014**, *136*, 6866–6869.
21. Corten, C. C.; Urban, M. W. Shape Evolution Control of Phase-Separated Colloidal Nanoparticles. *Polym. Chem.* **2011**, *2*, 244–250.
22. Schulz, S.; Gisler, T.; Borkovec, M.; Sticher, H. Surface Charge on Functionalized Latex Spheres in Aqueous Colloidal Suspensions. *J. Colloid Interface Sci.* **1994**, *164*, 88–98.
23. Stöber, W.; Fink, A.; Bohn, E. Controlled Growth of Monodisperse Silica Spheres in the Micron Size Range. *J. Colloid Interface Sci.* **1968**, *26*, 62–69.